Short article

The Hsf1-sHsp cascade has pan-antiviral activity in mosquitoes

Jieqiong Qu [1], Michelle Schinkel [1], Lisa Chiggiato [1], Samara Rosendo Machado [1], Gijs J. Overheul [1], Pascal Miesen [1], Ronald P. van Rij [1,2,*]

[1] Department of Medical Microbiology, Radboud Institute for Molecular Life Sciences, Radboud University Medical Center, P.O. Box 9101, 6500 HB Nijmegen, The Netherlands

[2] Lead contact

* Correspondence: Ronald.vanRij@radboudumc.nl

GRAPHICAL ABSTRACT

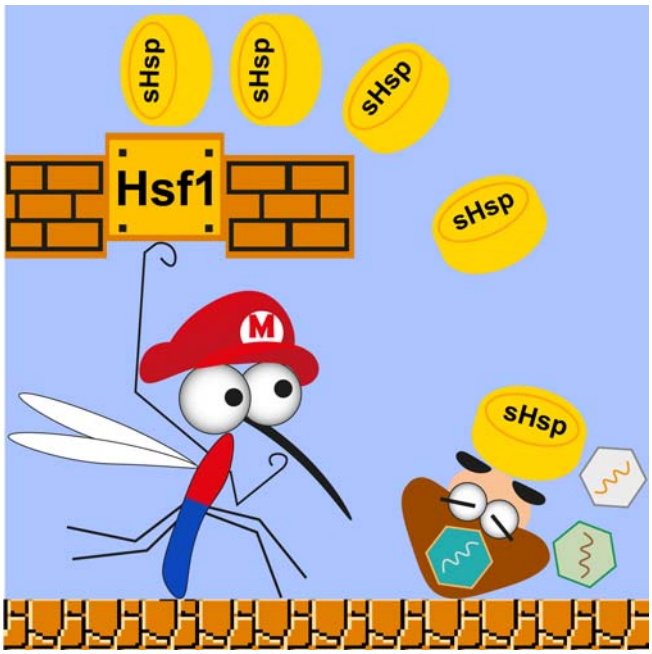

HIGHLIGHTS

- Hsf1 regulates eight sHsp genes within one topologically associated domain.
- The Hsf1-sHsp cascade functions as an early response against chikungunya virus infection.
- Broad antiviral activity of the Hsf1-sHsp cascade is conserved in three mosquito species.
- Hsf1 activation reduces the chikungunya virus infection rate in *Aedes aegypti* mosquitoes.

SUMMARY (133 words)

Aedes mosquitoes transmit pathogenic arthropod-borne (arbo) viruses, putting nearly half the world's population at risk. Blocking virus replication in mosquitoes is a promising approach to prevent arbovirus transmission, the development of which requires in-depth knowledge of virus-host interactions and mosquito immunity. By integrating multi-omics data, we find that heat shock factor 1 (Hsf1) regulates eight small heat shock protein (sHsp) genes within one topologically associated domain in the mosquito genome. This Hsf1-sHsp cascade acts as an early response against chikungunya virus (CHIKV) infection and shows pan-antiviral activity in three vector mosquitoes, *Aedes aegypti*, *Aedes albopictus*, and *Anopheles gambiae*. Importantly, activation of Hsf1 leads to a reduced CHIKV infection rate in adult *Ae. aegypti* mosquitoes, establishing Hsf1 as a promising target for the development of novel intervention strategies to limit arbovirus transmission by mosquitoes.

KEY WORDS

heat shock factor 1 (Hsf1), small heat shock protein (sHsp), antiviral immunity, topological associated domain (TAD), *Aedes aegypti*, mosquito, arbovirus, chikungunya virus (CHIKV), dengue virus (DENV), alphavirus

INTRODUCTION

Aedes mosquitoes are the primary vectors of arthropod-borne (arbo) viruses [1] that pose significant health and economic burden to humans [2-4]. Dengue virus (DENV) alone causes approximately 400 million infections and 20,000 deaths annually [5]. Recent outbreaks of chikungunya virus (CHIKV) in Europe and the Americas have also garnered significant attention [6-11]. With the continued resurgence of arboviruses and their unprecedented geographical spread over the past years, there is a pressing need for novel strategies to prevent and mitigate future outbreaks.

Arbovirus transmission occurs primarily through a horizontal cycle between blood-feeding arthropod vectors, such as mosquitoes, and vertebrate hosts. Female mosquitoes ingest viruses during a blood meal from an infected host and then transfer viruses into a naïve host through biting [12,13]. Blocking virus transmission at the mosquito stage, rather than solely targeting the virus in human hosts, constitutes a promising, alternative approach to prevent arbovirus spread [14]. The development of such approaches requires in-depth knowledge of mosquito antiviral immunity.

Our current understanding of the insect immune system is largely informed by studies in *Drosophila melanogaster* [15-18], where the RNA interference (RNAi) pathway serves as a major response that degrades viral RNA and inhibits replication [19,20]. Innate immune signaling pathways, specifically the NF-κB (Toll and IMD) and JAK-STAT pathways, have also been implicated in antiviral defense [16,21]. However, *Drosophila* does not recapitulate mosquito specific processes such as virus acquisition and transmission via blood-feeding [12,13,15,21]. It is therefore crucial to study immunity against arboviruses in relevant species, such as *Ae. aegypti*, the primary vector of the urban virus transmission cycle [22,23]. RNAi has been identified as a major antiviral response in *Ae. aegypti* mosquitoes, with evidence from CHIKV [24], ZIKV [25,26], DENV [27,28], and Sindbis virus (SINV) [29]. In contrast, the role of classical innate immune pathways is less well-defined and seems to be virus dependent [30-34]. For instance, ZIKV infection activates the Toll pathway, while DENV infection activates both the Toll and JAK-STAT pathways [30-32]. Activation of the Toll and JAK-STAT pathways by depleting pathway-specific negative regulators Cactus and PIAS, respectively, suppresses ZIKV infection [30]. On the other hand, activation of the IMD pathway by silencing of Caspar did not affect ZIKV infection [30], but impaired SINV replication [33]. Additionally, stimulation with either heat inactivated *E. coli* to activate JAK-

STAT and IMD pathways or *B. subtilis* to activate Toll pathway had no effect on CHIKV replication [24], suggesting unknown antiviral mechanisms yet to be discovered.

To investigate the transcriptional responses of *Ae. aegypti* to viral infection, we conducted a time-course RNA-seq experiment upon CHIKV infection. Our combined analyses of RNA-seq and chromatin profiling data revealed an early-responsive cascade, consisting of heat shock factor 1 (Hsf1) driving the expression of eight small heat shock proteins (sHsps). This Hsf1-sHsp cascade displayed pan-antiviral activities in three vector mosquitoes. Furthermore, activation of Hsf1 led to a reduced CHIKV infection rate *in vivo* in adult *Ae. aegypti* mosquitoes. As such, Hsf1 serves as a promising target for the development of new intervention strategies to control arbovirus transmission by mosquitoes.

RESULTS

The Hsf1-sHsp cascade acts as an early response to CHIKV infection

To uncover novel components involved in antiviral defense in *Aedes* mosquitoes, we performed a time-course RNA-seq experiment to determine differentially expressed genes (DEgenes) upon CHIKV infection of *Ae. aegypti* Aag2 cells at 4, 8 and 48 hours post-infection (hpi) (Figure 1A and Table S1). A high multiplicity of infection (MOI) of 5 was used to ensure that the vast majority of cells are synchronously infected and that DEgenes from different time points represent transcriptional responses at different stages of infection. At 4 hpi, only a single DEgene was detected (*AAEL000080*, encoding a putative phosphoenolpyruvate carboxykinase), which was also downregulated at 8 hpi. We observed major transcriptional changes at 8 hpi and 48 hpi, which we termed the early and late responses to CHIKV infection, respectively. The late response was more pronounced, with eight upregulated and 51 downregulated genes (Figure 1A), and KEGG pathway analysis suggested that downregulated DEgenes were mainly involved in glycolysis, which we have reported before [35]. In contrast, the early response was modest, with two downregulated and 19 upregulated genes, which were enriched for genes encoding HSP20-like chaperones (Figure 1A). Protein domain analysis revealed four heat shock protein 70 (Hsp70) and eight small heat shock proteins (sHsps) (Figure 1B), which function to prevent protein aggregation and to help cells to survive stressful conditions [36].

While Hsp70 is involved in distinct steps of the viral cycle, including entry, RNA replication, and virion assembly [37,38], the role of sHsps during virus infection is largely unknown [39]. Inspecting the genomic distribution of these sHsp genes, we found that all eight sHsps are encoded within one Topologically Associated Domain (TAD) deduced from Hi-C seq data [40] (Figure 1C), suggesting that these sHsp genes are coordinately regulated by a similar cis-regulatory network [41,42]. To further study the regulation of sHsp gene expression within this TAD, we mapped our chromatin profiling data from Aag2 cells [43], and performed motif scan within open chromatin regions defined by the Assay for Transposase-Accessible Chromatin with sequencing (ATAC-seq). We found the DNA binding motif of the transcription factor heat shock factor 1 (Hsf1) to be highly enriched at promoter regions of these eight sHsp genes, but not at other genes within the same TAD (Figure 1D). These regions were also marked by active histone marks H3K4me3 and H3K27ac, as well as RNA polymerase II occupancy, indicating active transcription. These findings together suggest that Hsf1 is the transcription factor that regulates sHsp gene expression. To experimentally test this hypothesis, we RNAi silenced *Hsf1*, and indeed, the induction of all eight *sHsps* upon CHIKV infection was significantly diminished (Figure 1E). Hence, the Hsf1-sHsp cascade functions as an early transcriptional response to CHIKV infection in Aag2 cells.

The Hsf1-sHsp cascade displays a broad antiviral activity

To explore the antiviral potential of the identified Hsf1-sHsp axis, we RNAi silenced *Hsf1* and observed elevated CHIKV RNA levels (Figure 2A). sHsp genes share high similarity at the nucleotide level, we therefore used two sets of dsRNA targeting the conserved Hsp20 domain to knock down sHsp expression and observed significantly increased CHIKV RNA copies (Figure 2B). In parallel, we knocked down *Hsp70*, which did not affect CHIKV replication (Figure 2C). These results together suggested that the Hsf1-sHsp axis has antiviral activity against CHIKV infection.

We then modulated the activity of Hsf1 with either the small molecule inhibitor KRIBB11 [44], or the activator hsfa1 [45]. KRIBB11 inhibits Hsf1-dependent recruitment of positive Transcription Elongation Factor b to the promoters of target genes, thus blocking gene activation [44]. Indeed, KRIBB11 treatment did not affect *Hsf1* expression, but led to more than 5-fold increase of viral RNA levels in Aag2 cells at 12 hpi of CHIKV infection (Figure 2D). The effect of KRIBB11 on virus replication remained concordant at 24 hpi. While the expression

of most *sHsps* was significantly reduced with KRIBB11 treatment, counterintuitively, we observed de-repression or even activation of some *sHsps*, such as *AAEL013346*, *AAEL013349*, and *AAEL013351* at 12 hpi, which is likely a secondary effect resulting from the increased CHIKV replication (Figure 2D). The precise mechanism by which hsfa1 activates Hsf1 is not yet understood [45]. We observed a significant increase in the *Hsf1* expression upon hsfa1 treatment, and accordingly a strong activation of all eight *sHsp* genes. Importantly, hsfa1 treatment led to about 25-fold reduction in CHIKV copies at 12 hpi and about 10-fold reduction at 24 hpi (Figure 2D), which is in agreement with our RNAi experiments and thus substantiates the antiviral role of sHsps.

Next, we tested the effect of these compounds on replication of other alphaviruses, including SINV (Figure 2E), the insect-specific Agua Salud alphavirus (ASALV, Figure 2F), and the flavivirus DENV (Figure 2G). Consistently, KRIBB11 treatment led to increased virus replication, whereas hsfa1 treatment significantly reduced virus replication (Figures 2E-G). We then extended our findings to other mosquito species and confirmed the antiviral property of the Hsf1-sHsp cascade in several natural virus-vector combinations, such as CHIKV in *Aedes albopictus* U4.4 cells (Figure 2H) and C6/36 cells (Figure 2I), and O'nyong-nyong (ONNV) in *Anopheles gambiae* Mos55 cells (Figure 2J). The fact that the heat shock response was antiviral in both U4.4 cells and the RNAi-deficient C6/36 cells indicates that the Hsf1-sHsps cascade functions independently of RNAi. Together, these results suggest that the newly defined Hsf1-sHsp pathway displays a pan-antiviral role in cells from all three tested mosquito species.

To identify which stage of the virus life cycle is affected by the Hsf1-sHsp cascade, we performed time-of-addition assays in Aag2 cells treated with either hsfa1 or KRIBB11 at different time points relative to inoculation with CHIKV at a high MOI (Figures 3A and S1A). When hsf1a was added at time points before inoculation up to 4 hpi, CHIKV replication was strongly inhibited (Figure 3B), indicating that hsfa1 does not affect the virus attachment or entry step. After 4 hpi, positive and negative sense viral RNA copies reached a detectable level and the inhibitory effect of hsf1a on CHIKV replication started to diminish gradually (Figures 3B), suggesting that the Hsf1-sHsp cascade interacts with the early stage of virus RNA replication. In agreement, time-of-addition assay with KRIBB11 treatment showed the same pattern (Figure S1).

To sum up, we demonstrated that the Hsf1-sHsp cascade displays a broad antiviral activity in mosquito cells,

likely via reducing early virus replication. As such, the upstream transcription factor, Hsf1, serves as a promising target for developing antiviral interventions in mosquitoes.

In vivo antiviral activity of the Hsf1-sHsp cascade

We next sought to determine the antiviral activity of the identified Hsf1-sHsp cascade in mosquitoes. Using RNA-seq, we first assessed the baseline expression of *sHsp* genes, which varied dramatically across different tissues of female *Ae. aegypti* (Figure 4A). Interestingly, *sHsp* genes were expressed at low levels in two main barrier tissues, the midgut and salivary glands, compared to other tissues such as the crop (Figure 4A).

We then assessed whether the Hsf1-sHsp cascade is activated as an antiviral response against CHIKV infection. We first established the *in vivo* CHIKV infection kinetics in *Ae. aegypti* mosquitoes (Figure S2A) and subsequently examined different tissues at 3 d and 5 d post blood feeding (dpf) when the virus had disseminated to most body parts (Figures S2B and C). Midguts and salivary glands showed comparable CHIKV RNA levels at 3 dpf, while salivary glands showed the highest CHIKV RNA levels at 5 dpf (Figure S2B). Despite relatively uniform CHIKV RNA levels, *sHsp* expression fluctuated within each tissue. Interestingly, a minor induction of some *sHsp* genes (*e.g.*, *AAEL013344*) was observed in ovaries, but not in other tissues (Figure S2C), suggesting that specific sHsps may play a protective role in ovaries.

We subsequently explored the possibility of activating Hsf1 in mosquitoes with small molecule compounds. However, due to the poor solubility of hsfa1 and KRIBB11 in blood, we could not continue with these two compounds in *in vivo* experiments. Instead, we tested another compound, Direct Targeted Hsf1 InhiBitor (DTHIB), which has been reported as a direct human Hsf1 inhibitor by stimulating the degradation of nuclear Hsf1 [46]. Unexpectedly, DTHIB treatment did not affect *Hsf1* expression but resulted in a dose-dependent activation of *sHsp* expression in Aag2 cells (Figures 4B-C). Thus, rather than an inhibitor, DTHIB acts as an Hsf1 activator in mosquito cells. Indeed, in line with our observations with hsf1a, treatment with DTHIB strongly reduced CHIKV replication in Aag2 cells (Figure 4B).

To assess the antiviral potential of the Hsf1-sHsp axis in vivo, 3-5 day-old *Ae. aegypti* female mosquitoes were fed with a CHIKV infectious blood meal in the presence of DTHIB or DMSO as a control. We assessed

the infectious titers at 3 dpf and did not observe a clear difference (Mann-Whitney test), however, there was a significant reduction in the infection rate, from 62% to 33%, with DTHIB treatment (Figure 4D), indicating that activation of Hsf1 presents a bottleneck to CHIKV infection in *Ae. aegypti* mosquitoes.

DISCUSSION

Our combined analyses of RNA-seq and epigenetic profiling revealed an early-responsive Hsf1-sHsp cascade that is activated upon CHIKV infection, which we found to have broad antiviral activity against alphaviruses and a flavivirus in three vector mosquito species: *Ae. aegypti*, *Ae. albopictus*, and *An. gambiae*. *In vivo* activation of Hsf1 resulted in a significant decrease in the CHIKV infection rate in *Ae. aegypti* mosquitoes. Overall, our work uncovers a novel antiviral cascade Hsf1-sHsp and identifies Hsf1 as a promising target for developing transmission-blocking strategies against arboviruses (Figure 4E).

While RNAi is a well-established antiviral mechanism in mosquito vectors, it is becoming evident that inducible signaling pathways are of vital importance as well. In addition to the classical Toll, IMD, and JAK-STAT pathways, Wnt, mTOR, Ras/ERK, c-jun pathways, and the Hsf1-sHsp cascade identified in this study, have been implicated in antiviral host defense [30,32,33,47-49]. The temporal activation of signaling pathways and associated genes is precisely regulated, as revealed by our time-course RNA-seq data. The activation of *sHsp* genes is mainly restricted to the early stage and is not detectable in the late stage of CHIKV infection. In line with our findings, published RNA-seq data from an *in vivo* study of *Ae. aegypti* mosquitoes showed a similar pattern, with a higher induction of *sHsp* expression at the early stage (3 dpi) than at the late stage (7 dpi) of CHIKV infection [39]. To gain deeper insights into the regulation of *sHsp* genes, we performed integrative analyses of 3D chromatin confirmation (Hi-C seq) and chromatin profiling data (ATAC-seq and ChIP-seq), and identified Hsf1 as the upstream transcription factor that regulates expression of eight *sHsp* genes within one TAD. Targeting the transcription factor Hsf1, rather than individual downstream genes, is expected to be more effective for antiviral control. Indeed, when we activated Hsf1 in adult mosquitoes, we observed a significant decrease in the CHIKV infection rate. Together, our multi-omics analysis strategy demonstrates its power in discovering novel antiviral signaling pathways, which can be applied to further investigate virus-vector interactions in different tissues, in other mosquito species, and in the context of other arboviruses.

While Hsp70 is required at various stages of the viral cycle including entry, RNA replication, and virion assembly [37,38,50,51], few studies analyzed the role of sHsps in viral infection [39]. This may be due to their transit activation pattern during the early stages of virus infection, making them difficult to capture. Indeed, we failed to observe robust induction of *sHsp* genes upon CHIKV blood feeding in different tissues, which is likely due to the asynchronous virus infection followed by asynchronous *sHsp* activation. In this case, single-cell RNA-seq may provide more insights into heterogeneity of gene expression. Moreover, *AAEL013344*, one of the *sHsp* genes, was found to be upregulated upon ZIKV infection [51], and further investigation is needed to assess whether *sHsp* genes are coordinately upregulated by specific arboviruses.

The mechanism underlying the antiviral activity of the Hsf1-sHsp cascade remains largely elusive. Our time-of-addition assays suggest that the response inhibits an early post-entry stage of the viral replication cycle. As Hsf1 activation led to a broad antiviral effect in three vector mosquitoes, it is likely that the Hsf1-sHsp cascade interacts, either directly or indirectly, with a common viral protein feature or a conserved host protein complex. It has been suggested that sHsps maintain protein homeostasis by binding proteins in non-native conformations, thereby preventing substrate aggregation [52]. The fact that a wide range of proteins is protected from precipitation suggests that sHsps may act rather promiscuously, similarly to the molecular chaperone Hsp70 [52-56]. It will be of great interest to profile sHsp associated proteins using proteomic approaches to identify sHsp client proteins and shed light on its antiviral mechanism.

To sum up, we identified the Hsf1-sHsp cascade as a novel antiviral mechanism in mosquitoes and propose Hsf1 as a promising target for developing arbovirus-blocking interventions. Considering the pan-antiviral activity of the Hsf1-sHsp cascade, our findings open the way for the development of a broad-spectrum drug to prevent arbovirus transmission.

ACKNOWLEDGEMENTS

We thank Martijn van Hemert (Leiden University Medical Center), Sandra Junglen (Charité Universitätsmedizin Berlin), Andres Merits (University of Tartu), Beate Kümmerer (University of Bonn), and Jason Rasgon (Pennsylvania State University) for providing materials. We thank BEI resources established by the National Institute of Allergy and Infectious Diseases for providing *Aedes aegypti* Liverpool mosquitoes. We thank Benoit Besson, Finny Varghese, and other members of the laboratory for fruitful discussions. This work is supported by a VENI grant from the Dutch Research Council to P.M. (grant number VI.Veni.202.035) and a VICI grant from the Dutch Research Council to R.P.v.R. (grant number 016.VICI.170.090).

AUTHOR CONTRIBUTIONS

J.Q., P.M., and R.P.v.R designed the experiments and analyzed the data. J.Q. performed computational analyses. J.Q., M.S., L.C., S.R.M., and G.O., performed the experiments. J.Q. and R.P.v.R. wrote the paper. All authors read and contributed to the manuscript.

DECLARATION OF INTERESTS

The authors declare no competing interests.

MAIN FIGURE TITLES AND LEGENDS

Figure 1. Hsf1 activates sHsps during the early stage of CHIKV infection.

(A) Hierarchical clustering of differentially expressed (DE) genes at 4, 8, and 48 hpi of CHIKV infection (MOI = 5), as quantified from RNA-seq data. DEgenes ($p < 0.05$) at each time point are color labeled on the left; KEGG pathway and InterPro enrichment is shown on the right. Z scores were calculated based on log-transformed Fragments per Kilobase per Million mapped reads (FPKM).

(B) Gene structure and protein domain analysis of heat shock proteins upregulated at 8 hpi of CHIKV infection. A neighbor-joining tree was constructed based on amino acid sequences (left). The $\log_2$ fold change in gene expression was quantified by RNA-seq (middle). The gene structure and InterPro protein domains are shown along the gene body (right).

(C) Hi-C interaction track with topologically associated domains (TADs) shown as horizontal blue bars ($p < 0.05$).

(D) Genome browser tracks showing RNA-seq data of mock and CHIKV infected Aag2 cells and chromatin profiling data from uninfected Aag2 cells (ATAC-seq, histone marks and RNA pol II ChIP-seq) within the indicated TAD. Eight upregulated *sHsp* genes at 8 hpi are highlighted in orange, other genes in gray. Predicted Hsf1 motifs are shown as green arrowheads at the bottom.

(E) Expression of the indicated genes in CHIKV (MOI = 5) (+) or mock (-) infected Aag2 cells upon RNAi-mediated silencing of *Hsf1* at 8 hpi . Luciferase dsRNA served as a non-targeting control (ctr). RT-qPCR was performed in biological quintuplicates and shown as dots, with horizontal lines and the bars indicating mean ± SD. Symbols denote statistical significance in unpaired t-tests (ns, not significant, * $p < 0.05$, ** $p < 0.01$, *** $p < 0.001$).

Figure 2. Pan-antiviral activity of the Hsf1-sHsp axis

(A-C) RNAi silencing of *Hsf1* (A), *sHsps* (B), *Hsp70* (*AAEL017975*) (C), and quantification of CHIKV RNA copies. RT-qPCR was used to assess target gene knockdown in uninfected Aag2 cells (left) and to quantify CHIKV mRNA copies at 8 hpi (MOI = 5) after target gene knockdown (right) in biological triplicate or quadruplicate, with luciferase dsRNA (dsLuc) serving as a non-targeting control. Original data are shown as dots, with bars indicating mean ± SD. Symbols denote statistical significance in unpaired t-tests (ns, not significant, * $p < 0.05$, ** $p < 0.01$, *** $p < 0.001$).

(D) Treatment with either Hsf1 inhibitor KRIBB11 (10 μM) or Hsf1 activator hsfa1 (100 μM). RT-qPCR was performed to analyze the expression of *Hsf1* (left), *sHsps* (middle), and changes in CHIKV RNA copies (right) at 12 and 24 hpi of CHIKV (MOI = 5), with DMSO serving as a control.

(E-G) Viral RNA levels in Aag2 cells treated with KRIBB11 (10 μM) or hsfa1 (100 μM) at 12 hpi of Sindbis

virus (SINV, MOI = 5) (E), at 12 hpi of Agua Salud alphavirus (ASALV, MOI = 5) (F), and at 72 hpi of dengue virus (DENV, MOI = 0.01) (G).

(H-J) Viral RNA levels upon treatment with KRIBB11 (5 μM) and hsfa1 (100 μM) at 12 hpi of CHIKV (MOI = 5) in U4.4 cells (H), at 12 hpi of CHIKV (MOI = 5) in C6/36 cells (I), at 48 hpi of o'nyong'nyong virus (ONNV, MOI = 0.5) in Mos55 cells (J). RT-qPCR was performed in biological quadruplicate or sextuplicate, shown as dots, with the bars indicating mean ± SD. Symbols denote statistical significance in unpaired t-tests (ns, not significant, * $p < 0.05$, ** $p < 0.01$, *** $p < 0.001$).

Figure 3. hsfa1 inhibits the early stage of CHIKV replication

(A) Schematic illustration of the time-of-addition assay, with hsfa1 added at different time points during CHIKV infection (MOI = 5). Cell culture medium was refreshed to wash away unbound virus particles at 1 hpi. Cells treated with either hsfa1 (orange) or DMSO (gray) were harvested at each indicated time point.

(B) The effect of hsfa1 (100 μM) on virus replication was determined with RT-qPCR on both positive sense RNA (+, left) and negative sense RNA (-, right). Data are presented as means ± SD of three independent experiments, with DMSO serving as control.

Figure 4. Antiviral activity of the Hsf1-sHsp axis *in vivo*

(A) Genome browser tracks of RNA-seq showing the expression of *sHsp* genes in the indicated tissues.

(B) Relative *Hsf1* expression and CHIKV RNA copies by RT-qPCR in Aag2 cells upon DTHIB treatment at 12 hpi of CHIKV (MOI = 5) in biological triplicates, shown as dots. A series of DTHIB concentrations were tested and is shown in different colors. Symbols denote statistical significance in one-way ANOVA (** $p < 0.01$, *** $p < 0.001$).

(C) Relative *sHsp* expression to the house-keeping gene *LAP* by RT-qPCR in Aag2 cells upon DTHIB treatment at 12 hpi of CHIKV (MOI = 5) in biological triplicates, shown as dots. A series of DTHIB concentrations were tested and is shown in different colors. Trend lines of the mean of three independent experiments were plotted.

(D) Mosquito CHIKV infection status at 3 dpf with DTHIB treatment. 3-5 day-old *Ae. aegypti* female mosquitoes were fed with blood containing CHIKV and DTHIB (0.4 mM, orange) or DMSO as a control (white). For virus titer comparison, Mann-Whitney test was performed (ns, not significant). The infection rate of whole mosquitoes from each group was plotted as pie charts and compared using Chi-squared test, with the *p* value labeled.

(E) A working model for the antiviral activity of the Hsf1-sHsp cascade in mosquitoes.

SUPPLEMENTARY FIGURE TITLES AND LEGENDS

Figure S1. The time-of-addition assay of KRIBB11, related to Figure 3

(A) Schematic illustration of the time-of-addition assay, with KRIBB11 added at different time points during CHIKV infection (MOI=5). Cell culture medium was refreshed to wash away unbound virus particles at 1 hpi. Cells treated with either KRIBB11 (dark gray) or DMSO (gray) were harvested at each indicated time point.
(B) The effect of KRIBB11 (10 μM) on virus replication was determined with RT-qPCR on both positive sense RNA (+, left) and negative sense RNA (-, right). Data are presented as means ± SD of three independent experiments, with DMSO serving as control.

Figure S2. Inspection of *sHsp* gene expression in different tissues, related to Figure 4.

(A) *in vivo* CHIKV infection kinetics. 3-5 day-old *Ae. aegypti* female mosquitoes were fed with CHIKV infectious blood. At the indicated time points, head, thorax, abdomen, and legs from individual mosquitoes were dissected and used for titration. Number of mosquitoes per time point are indicated on top.
(B-C) CHIKV levels in midguts, Malpighian tubules, ovaries and salivary glands at 3 d and 5 d after infectious blood meal. RT-qPCR was performed to quantify CHIKV RNA copies (B) and expression of *sHsp* genes (C). Dissected organs from 15 mosquitoes were pooled as one sample and shown as one dot. Data are presented as mean values ± SD of three biological replicates. Mock infections are shown as white symbols and bars, CHIKV infections as orange symbols and grey bars.

316 KEY RESOURCES TABLE

REAGENT or RESOURCE	SOURCE	IDENTIFIER
Bacterial and virus strains		
CHIKV expression plasmid encoding the Leiden synthetic (LS3) wildtype strain	Kindly provided by Dr. M.J. van Hemert (Leiden University Medical Center) [57]	GenBank: JX911334.1
SINV expression vector pTE3' 2J	[58]	strain AR339
ASALV strain PA-2013-MP416	Kindly provided by Sandra Junglen (Charité, Berlin) [59]	GenBank: MK959114
ONNV	Kindly provided by Andres Merits (University of Tartu)	N/A
DENV2, strain 16681	Kindly provided by Beate Kümmerer (University of Bonn)	strain 16681
Critical commercial assays		
X-tremeGENE HP DNA Transfection Reagent	Roche	6366546001
TaqMan Reverse Transcription Reagents	Invitrogen	N8080234
GoTaq qPCR Master Mix	Promega	A6002
mMESSAGE mMACHINE™ T7 Transcription Kit	Invitrogen	AM1344
TruSeq Stranded mRNA kit	Illumina	20020594
High Sensitivity DNA Chip	Agilent	5067-4626
Chemicals, peptides, and recombinant proteins		
Leibovitz's L-15 medium	Gibco	21083-027
Schneider's insect medium	Gibco	21720024
Dulbecco's Modified Eagle Medium (DMEM)	Gibco	41965039
Fetal bovine serum	Sigma	F7524-500ML
Penicillin/Streptomycin	Gibco	15070-063
Non-essential amino acids	Gibco	11140-035
Tryptose phosphate broth solution	Sigma	T8159-100ML
KRIBB11	Axon Medchem	2538
Hsf1a	Axon Medchem	1890
DTHIB	Axon Medchem	3412
Deposited data		
Time-course CHIKV infection RNA-seq data	[35]	PRJNA885496
Hi-C seq	[40]	GSE95797
Chromatin profiling data	[43]	GSE210270
Mosquito tissue RNA-seq	This study	GSE225070
Experimental models: Cell lines		
Ae. aegypti Aag2 cells	Kindly provided by Raul Andino (University of California San Francisco) [60]	https://doi.org/10.1016/0042-6822(68)90293-6
Ae. albopictus U4.4 cells	Kindly provided by Gorben Pijlman (Wageningen University)	N/A
Ae. albopictus C6/36 cells	ECACC General Cell Collection	#89051705

An. gambiae Mos55 cells	Kindly provided by Jason L. Rasgon from The Pennsylvania State University [61]	N/A
Baby hamster kidney cells (BHK-21)	N/A	RRID: CVCL_1914
BHK-21 clone 15 (BHK-15)	[62]	N/A
Experimental models: Organisms/strains		
Ae. aegypti mosquitoes	Obtained from BEI resources	Black Eye Liverpool strain
Oligonucleotides		
PCR and qPCR primers, see Table S2	Thermo Fisher scientific	N/A
Software and algorithms		
FastQC	[63]	https://www.bioinformatics.babraham.ac.uk/projects/fastqc/
STAR	[64]	https://github.com/alexdobin/STAR
Cuffdiff	[65]	https://chipster.csc.fi/manual/cuffdiff2.html
deepTools	[66]	https://deeptools.readthedocs.io/en/develop/
DESeq2	[67]	http://bioconductor.org/packages/devel/bioc/vignettes/DESeq2/inst/doc/DESeq2.html
pheatmap	[68]	RRID: SCR_016418
STRING	[69]	https://string-db.org/
InterPro	[70]	https://www.ebi.ac.uk/interpro/
HiCExplorer	[71]	https://hicexplorer.readthedocs.io/en/latest/
MACS2	[72]	https://hbctraining.github.io/Intro-to-ChIPseq/lessons/05_peak_calling_macs.html
Homer	[73]	http://homer.ucsd.edu/homer/motif/
GraphPad Prism 9	GraphPad	https://www.graphpad.com/scientific-software/prism/

317

STAR METHODS

RESOURCE AVAILABILITY

Lead contact

Further information and requests for resources and reagents should be directed to the lead contact, Ronald P. van Rij (Ronald.vanRij@radboudumc.nl).

Materials availability

This study did not generate new unique reagents.

Data and code availability

- Newly generated sequencing data have been deposited at GEO (GSE225070) and will be publicly available at the date of publication. This paper analyzes existing, publicly available data. The accession numbers for the datasets are listed in the Key Resources Table.
- This paper does not report original code.
- Any additional information required to reanalyze the data reported in this paper is available from the lead contact upon request.

EXPERIMENTAL MODEL AND SUBJECT DETAILS

Cell lines

Ae. aegypti Aag2 cells, *Ae. albopictus* U4.4 and C6/36 cells were grown in Leibovitz's L-15 medium supplemented with 10% fetal bovine serum, 50 U/ml Penicillin, 50 µg/mL Streptomycin, 1x non-essential Amino Acids and 2% Tryptose phosphate broth solution. *An. gambiae* Mos55 cells were grown in Schneider's insect medium supplemented with 10% fetal bovine serum, 50 U/ml Penicillin, and 50 µg/mL Streptomycin. These cell lines were cultured at 28°C without CO_2.

BHK-15 and BHK-21 cells were grown in Dulbecco's modified Eagle medium (DMEM), supplemented with 10% foetal bovine serum, 50 U/mL penicillin, and 50 µg/mL streptomycin. These mammalian cells were cultured at 37°C, with 5% CO_2.

Viruses

The CHIKV expression plasmid encoding the Leiden synthetic (LS3) wildtype strain was kindly provided by Dr. M.J. van Hemert (Leiden University Medical Center) and viral RNA was obtained by *in vitro* transcription on linearized plasmids using T7 mMessage mMachine (Invitrogen) [57]. RNA was then transfected into BHK-21 to grow the infectious virus. SINV AR339 strain (pTE3' 2J) was obtained by transfecting *in vitro* transcribed RNA from pTE3' 2J in BHK-21 cells [58]. ASALV, kindly provided by Sandra Junglen (Charité, Berlin), was originally isolated from the homogenate of mosquito pool MP416 and grown in C6/36 cells [59]. ONNV plasmid was kindly provided by Prof. Dr. Andres Merits (University of Tartu), *in vitro* transcribed and grown in C6/36 cells [74]. DENV serotype 2 (DENV2, strain 16681) was provided by Beate Kümmerer (University of Bonn) and stocks were prepared on C6/36 cells. For the quantification of viral stocks, CHIKV, SINV, and ONNV were titrated by end-point dilution on BHK-21 cells, DENV2 was titrated on BHK-15 cells,

and ASALV was titrated on C6/36 cells. A day before the titration, $1x10^4$ mammalian or $5x10^4$ C6/36 cells were seeded per well in a 96-well flat bottom plate. A 10-fold serial dilution of virus samples was added to the cells in quadruplicate for the titration. After an incubation time of 5 days, cells were inspected for cytopathic effect. The virus titer was calculated according to the Reed and Muench method [75].

Mosquito experiment

Ae. aegypti mosquitoes (Black Eye Liverpool strain, obtained from BEI Resources) were reared at 28 °C, with 70% humidity and automated room lighting set at a 12:12 hours light/dark cycle. Larvae were fed with Tetramin Baby fish food (Tetra). Adult mosquitoes were fed with a 10% sucrose solution. Three to five day-old female mosquitoes were used for experiments unless stated otherwise.

For blood feeding experiments, mosquitoes were starved for 24 h prior to the experiment. CHIKV virus stock (5×10^8 $TCID_{50}$/mL) and full human blood (Sanquin) was 1:2 mixed to make the infectious blood meal with a final virus titer of 1.7×10^8 $TCID_{50}$/ml. DMEM medium was mixed in the same ratio with human blood to prepare the mock inoculum. Blood feeding was performed with the Hemotek system for half an hour. Afterwards, mosquitoes were anesthetized on a CO_2 pad. Only blood fed mosquitoes were selected and kept in culture until the indicated time points. Mosquitoes were tissue dissected as previously described [76]. Whole mosquitoes, dissected body parts or tissues were homogenized in either 200 µl DMEM medium for end-point titration on BHK-21 cells or in 1 mL RNA-Solv reagent (Omega Bio-Tek) for RNA isolation, using a Precellys 24 homogenizer program 5 (Bertin technologies).

METHOD DETAILS

RNAi in mosquito cells

PCR products flanked by T7 promoter sequences at both ends were *in vitro* transcribed by T7 polymerase to produce dsRNA. These PCR products were *in vitro* transcribed using a homemade T7 RNA polymerase. For the formation of double-stranded RNA, the reactions were heated to 90 °C for 10 minutes and then allowed to gradually cool to room temperature and RNA was purified using the GenElute Mammalian Total RNA kit (Sigma) according to the manufacturer's protocol. Two sets of dsRNA targeting the Hsp20 domain were used to knock down *sHsp* expression (Figure 2B) and two sets of dsRNA targeting the Hsp70 domain were used to knock down *Hsp70* (Figure 2C). For detailed oligonucleotide information, see Table S2.

Aag2 cells were seeded at a density of $1.5x10^5$ cells/well in a 24-well plate, 24 h before the dsRNA transfection. For each target gene, a transfection mix containing 300 µl non-supplemented L-15 medium, 500 ng dsRNA, and 1.3 µl X-treme GENE HP DNA transfection reagent (Sigma) was prepared according to the manufacturer's recommendations. Per well, 100 µl of the transfection mix was added in a dropwise manner. Cell culture medium was refreshed at 4 h post-transfection. Three days post-transfection, cells were either harvested for evaluation of target gene knockdown or infected with CHIKV at a MOI of 5.

RNA isolation and RT-qPCR

Aag2 cells were homogenized in RNA-Solv reagent (Omega Bio-Tek) and RNA extraction was performed according to the manufacturer's instructions. Briefly, 200 µl of chloroform was added to 1 mL RNA-Solv reagent, and thoroughly mixed. After centrifugation, the aqueous phase was collected, and RNA was precipitated using isopropanol. This mix was incubated for 1 hour at 4 °C followed by centrifugation to pellet the RNA. Pellets were washed twice in 80% ethanol, and dissolved in nuclease free water. RNA integrity was evaluated on ethidium bromide stained agarose gels, and RNA concentration was determined using the Nanodrop ND-1000.

For RT-qPCR analyses, DNaseI (Ambion)-treated RNA was reverse transcribed with random hexamers using the TaqMan Reverse Transcription Reagents (Invitrogen) and PCR amplified using the GoTaq qPCR system (Promega) on a LightCycler 480 (Roche). In RNAi experiments, expression levels of target genes were normalized to the expression of the housekeeping gene *lysosomal aspartic protease* (*LAP*, *AAEL006169*), and fold changes were calculated using the 2-ΔΔCT method [77]. All primers are listed in Table S2.

RNA-seq library preparation and analysis

For RNA sequencing in Aag2 cells, control dsRNA (dsLuc) treated cells were infected with CHIKV at a MOI of 5. The double stranded RNA treatment was included in the procedure to allow a better comparison of the 4 hpi and 8 hpi samples to the 48 hpi datasets that was generated in parallel for a previously published study [35].

Three to five day-old female mosquitoes were anesthetized on a CO_2 pad, washed once in 70% ethanol and three times with 1× PBS for outer de-contamation. Afterwards, crop, fat body, leg, Malpighian tubules, midgut, ovary, salivary glands, and wings were dissected. Tissues from about 20 mosquitoes were pooled to achieve enough RNA (1 µg) for RNA-seq library preparation. Three batches of mosquitoes were dissected and the corresponding RNA samples serve as biological triplicates for RNA-seq. TruSeq Stranded mRNA kit (Illumina) was used for library preparation from total RNA according to the manufacturer's protocol. The prepared libraries were quantified and controlled for sample quality using High Sensitivity DNA Chip on a DNA1000 Bioanalyzer (Agilent), and the libraries were analyzed on an Illumina HiSeq 4000 sequencer (GenomEast Platform).

After initial quality control by FastQC [63], raw sequence reads were aligned to the reference genome, *Ae. aegypti* LVP (Vectorbase, release 56), using STAR [64] with default settings. Quantification of gene expression (FPKM) was performed with Cuffdiff [65]. R package DESeq2 was used for differential gene expression analysis (with adjusted p value < 0.05) [67]. Genes were considered expressed if the mean of the DESeq2-normalized counts (basement) was higher than 20. The R package pheatmap was used to generate the heatmap for DEgenes upon CHIKV infection, which was based on z-scores of normalized gene expressions ($\log_{10}$ FPKM) [68]. DEgenes are listed in Table S1.

Bioinformatic analyses

STRING was used for KEGG pathway and InterPro protein domain enrichment analysis [69]. Detailed protein domain analysis was performed using InterPro [70].

For 3D chromatin confirmation analysis, TADs were defined by analyzing Hi-C data [40] with HiCExplorer [71]. A cut off of p < 0.05 was used, after correcting for multiple tests. pyGenomeTracks from the deepTools package [66] was used to visualize gene expression pattern, TADs, and previously published chromatin profiling data from Aag2 cells, including ATAC-seq, histone mark ChIP-seq and RNA pol II ChIP-seq [43]. All genome browser tracks were normalized to FPKM (y-axis). Open chromatin regions were defined as ATAC-seq peaks called by MACS2 with standard settings and a q value of 0.05 [72]. Homer was used for DNA motif scan on ATAC-seq peaks [73].

Compound experiment

KRIBB11 (2538), Hsf1a (1890), and DTHIB (3412) were purchased from Axon Medchem. All compounds were dissolved in DMSO to final concentrations of 10 mM (KRIBB11) or 100 mM (Hsf1a and DTHIB) and stored at 4°C for use within one month. Mosquito cells were seeded at a density of 1.5×10^5 cells/well in a 24-well plate. When cells reach 50% confluency, cells were treated with the indicated concentrations of

compound or an equivalent volume of DMSO and immediately afterwards inoculated with virus at the indicated MOI. Cell lysates were collected at indicated time points post-infection for RT-qPCR. For the time-of-addition assay, the same procedures were followed, except that the medium was replaced at 1 hpi. For mosquito experiments, compound was directly added to infectious blood meal and mixed well before blood feeding, with DMSO serving as a control.

QUANTIFICATION AND STATISTICAL ANALYSIS

For RT-qPCR experiments in Figures 1E and 2 were performed in biological triplicate, quintuplicate, or sextuplicate, with individual data shown as dots and the bars indicating mean ± SD. Statistical differences were examined by unpaired t-test. For RT-qPCR in Figure 4B, one-way ANOVA was performed. For virus titer comparison in Figure 4D, nonparametric Mann-Whitney U test was performed. For the infection rate comparison in Figure 4D, Chi-squared test was performed. All statistical significance in this study were produced by GraphPad Prism 9.

REFERENCES

1. Souza-Neto, J.A., Powell, J.R., and Bonizzoni, M. (2019). Aedes aegypti vector competence studies: A review. Infection, Genetics and Evolution *67*, 191-209.
2. Diagne, C., Leroy, B., Vaissière, A.-C., Gozlan, R.E., Roiz, D., Jarić, I., Salles, J.-M., Bradshaw, C.J., and Courchamp, F. (2021). High and rising economic costs of biological invasions worldwide. Nature, 1-6.
3. Weaver, S.C., and Reisen, W.K. (2010). Present and future arboviral threats. Antiviral research *85*, 328-345.
4. Chibueze, E.C., Tirado, V., da Silva Lopes, K., Balogun, O.O., Takemoto, Y., Swa, T., Dagvadorj, A., Nagata, C., Morisaki, N., and Menendez, C. (2017). Zika virus infection in pregnancy: a systematic review of disease course and complications. Reproductive health *14*, 1-14.
5. Brady, O.J., and Hay, S.I. (2020). The global expansion of dengue: how Aedes aegypti mosquitoes enabled the first pandemic arbovirus. Annual review of entomology *65*, 191-208.
6. Paty, M., Six, C., Charlet, F., Heuzé, G., Cochet, A., Wiegandt, A., Chappert, J., Dejour-Salamanca, D., Guinard, A., and Soler, P. (2014). Large number of imported chikungunya cases in mainland France, 2014: a challenge for surveillance and response. Eurosurveillance *19*, 20856.
7. Venturi, G., Di Luca, M., Fortuna, C., Remoli, M.E., Riccardo, F., Severini, F., Toma, L., Del Manso, M., Benedetti, E., and Caporali, M.G. (2017). Detection of a chikungunya outbreak in Central Italy, August to September 2017. Eurosurveillance *22*, 17-00646.
8. Burt, F.J., Chen, W., Miner, J.J., Lenschow, D.J., Merits, A., Schnettler, E., Kohl, A., Rudd, P.A., Taylor, A., and Herrero, L.J. (2017). Chikungunya virus: an update on the biology and pathogenesis of this emerging pathogen. The Lancet Infectious Diseases *17*, e107-e117.
9. Tomasello, D., and Schlagenhauf, P. (2013). Chikungunya and dengue autochthonous cases in Europe, 2007–2012. Travel medicine and infectious disease *11*, 274-284.
10. Calba, C., Guerbois-Galla, M., Franke, F., Jeannin, C., Auzet-Caillaud, M., Grard, G., Pigaglio, L., Decoppet, A., Weicherding, J., and Savaill, M.-C. (2017). Preliminary report of an autochthonous chikungunya outbreak in France, July to September 2017. Eurosurveillance *22*, 17-00647.
11. Rocklöv, J., Tozan, Y., Ramadona, A., Sewe, M.O., Sudre, B., Garrido, J., de Saint Lary, C.B., Lohr, W., and Semenza, J.C. (2019). Using big data to monitor the introduction and spread of chikungunya, Europe, 2017. Emerging infectious diseases *25*, 1041.
12. Farjana, T., and Tuno, N. (2013). Multiple blood feeding and host-seeking behavior in Aedes aegypti and Aedes albopictus (Diptera: Culicidae). Journal of medical entomology *50*, 838-846.
13. Manore, C.A., Ostfeld, R.S., Agusto, F.B., Gaff, H., and LaDeau, S.L. (2017). Defining the risk of Zika and chikungunya virus transmission in human population centers of the eastern United States. PLoS neglected tropical diseases *11*, e0005255.
14. Baldacchino, F., Caputo, B., Chandre, F., Drago, A., della Torre, A., Montarsi, F., and Rizzoli, A. (2015). Control methods against invasive Aedes mosquitoes in Europe: a review. Pest management science *71*, 1471-1485.
15. Merkling, S.H., and van Rij, R.P. (2013). Beyond RNAi: antiviral defense strategies in Drosophila and mosquito. Journal of insect physiology *59*, 159-170.
16. Mussabekova, A., Daeffler, L., and Imler, J.-L. (2017). Innate and intrinsic antiviral immunity in Drosophila. Cellular and Molecular Life Sciences *74*, 2039-2054.
17. Kingsolver, M.B., Huang, Z., and Hardy, R.W. (2013). Insect antiviral innate immunity: pathways, effectors, and connections. Journal of molecular biology *425*, 4921-4936.

492 18. Machado, S.R., van der Most, T., and Miesen, P. (2021). Genetic determinants of antiviral immunity
493 in dipteran insects–Compiling the experimental evidence. Developmental & Comparative
494 Immunology *119*, 104010.
495 19. Van Rij, R.P., Saleh, M.-C., Berry, B., Foo, C., Houk, A., Antoniewski, C., and Andino, R. (2006). The
496 RNA silencing endonuclease Argonaute 2 mediates specific antiviral immunity in Drosophila
497 melanogaster. Genes & development *20*, 2985-2995.
498 20. Wang, X.-H., Aliyari, R., Li, W.-X., Li, H.-W., Kim, K., Carthew, R., Atkinson, P., and Ding, S.-W. (2006).
499 RNA interference directs innate immunity against viruses in adult Drosophila. Science *312*, 452-454.
500 21. Tafesh-Edwards, G., and Eleftherianos, I. (2020). Drosophila immunity against natural and
501 nonnatural viral pathogens. Virology *540*, 165-171.
502 22. Vega-Rúa, A., Zouache, K., Girod, R., Failloux, A.-B., and Lourenço-de-Oliveira, R. (2014). High level
503 of vector competence of Aedes aegypti and Aedes albopictus from ten American countries as a
504 crucial factor in the spread of Chikungunya virus. Journal of virology *88*, 6294-6306.
505 23. Coffey, L.L., Failloux, A.-B., and Weaver, S.C. (2014). Chikungunya virus–vector interactions. Viruses
506 *6*, 4628-4663.
507 24. McFarlane, M., Arias-Goeta, C., Martin, E., O'Hara, Z., Lulla, A., Mousson, L., Rainey, S.M., Misbah,
508 S., Schnettler, E., and Donald, C.L. (2014). Characterization of Aedes aegypti innate-immune
509 pathways that limit Chikungunya virus replication. PLoS Negl Trop Dis *8*, e2994.
510 25. Buchman, A., Gamez, S., Li, M., Antoshechkin, I., Li, H.-H., Wang, H.-W., Chen, C.-H., Klein, M.J.,
511 Duchemin, J.-B., and Paradkar, P.N. (2019). Engineered resistance to Zika virus in transgenic Aedes
512 aegypti expressing a polycistronic cluster of synthetic small RNAs. Proceedings of the National
513 Academy of Sciences *116*, 3656-3661.
514 26. Magalhaes, T., Bergren, N.A., Bennett, S.L., Borland, E.M., Hartman, D.A., Lymperopoulos, K., Sayre,
515 R., Borlee, B.R., Campbell, C.L., and Foy, B.D. (2019). Induction of RNA interference to block Zika
516 virus replication and transmission in the mosquito Aedes aegypti. Insect biochemistry and
517 molecular biology *111*, 103169.
518 27. Franz, A.W., Sanchez-Vargas, I., Adelman, Z.N., Blair, C.D., Beaty, B.J., James, A.A., and Olson, K.E.
519 (2006). Engineering RNA interference-based resistance to dengue virus type 2 in genetically
520 modified Aedes aegypti. Proceedings of the National Academy of Sciences *103*, 4198-4203.
521 28. Sánchez-Vargas, I., Scott, J.C., Poole-Smith, B.K., Franz, A.W., Barbosa-Solomieu, V., Wilusz, J.,
522 Olson, K.E., and Blair, C.D. (2009). Dengue virus type 2 infections of Aedes aegypti are modulated by
523 the mosquito's RNA interference pathway. PLoS Pathog *5*, e1000299.
524 29. Khoo, C.C., Piper, J., Sanchez-Vargas, I., Olson, K.E., and Franz, A.W. (2010). The RNA interference
525 pathway affects midgut infection-and escape barriers for Sindbis virus in Aedes aegypti. BMC
526 microbiology *10*, 1-12.
527 30. Angleró-Rodríguez, Y.I., MacLeod, H.J., Kang, S., Carlson, J.S., Jupatanakul, N., and Dimopoulos, G.
528 (2017). Aedes aegypti molecular responses to Zika virus: modulation of infection by the toll and
529 jak/stat immune pathways and virus host factors. Frontiers in microbiology *8*, 2050.
530 31. Xi, Z., Ramirez, J.L., and Dimopoulos, G. (2008). The Aedes aegypti toll pathway controls dengue
531 virus infection. PLoS Pathog *4*, e1000098.
532 32. Behura, S.K., Gomez-Machorro, C., Harker, B.W., Debruyn, B., Lovin, D.D., Hemme, R.R., Mori, A.,
533 Romero-Severson, J., and Severson, D.W. (2011). Global cross-talk of genes of the mosquito Aedes
534 aegypti in response to dengue virus infection. PLoS Negl Trop Dis *5*, e1385.
535 33. Barletta, A.B.F., Nascimento-Silva, M.C.L., Talyuli, O.A., Oliveira, J.H.M., Pereira, L.O.R., Oliveira, P.L.,
536 and Sorgine, M.H.F. (2017). Microbiota activates IMD pathway and limits Sindbis infection in Aedes
537 aegypti. Parasites & vectors *10*, 1-9.

538 34. Souza-Neto, J.A., Sim, S., and Dimopoulos, G. (2009). An evolutionary conserved function of the
539 JAK-STAT pathway in anti-dengue defense. Proceedings of the National Academy of Sciences *106*,
540 17841-17846.
541 35. Machado, S.R., Qu, J., Koopman, W.J.H., and Miesen, P. (2022). The DEAD-box RNA helicase Dhx15
542 controls glycolysis and arbovirus replication in Aedes aegypti mosquito cells. bioRxiv,
543 2022.2006.2022.497281. 10.1101/2022.06.22.497281.
544 36. Garrido, C., Paul, C., Seigneuric, R., and Kampinga, H. (2012). The small heat shock proteins family:
545 the long forgotten chaperones. The international journal of biochemistry & cell biology *44*, 1588-
546 1592.
547 37. Taguwa, S., Maringer, K., Li, X., Bernal-Rubio, D., Rauch, J.N., Gestwicki, J.E., Andino, R., Fernandez-
548 Sesma, A., and Frydman, J. (2015). Defining Hsp70 subnetworks in dengue virus replication reveals
549 key vulnerability in flavivirus infection. Cell *163*, 1108-1123.
550 38. Taguwa, S., Yeh, M.-T., Rainbolt, T.K., Nayak, A., Shao, H., Gestwicki, J.E., Andino, R., and Frydman,
551 J. (2019). Zika virus dependence on host Hsp70 provides a protective strategy against infection and
552 disease. Cell reports *26*, 906-920. e903.
553 39. Wimalasiri-Yapa, B.R., Barrero, R.A., Stassen, L., Hafner, L.M., McGraw, E.A., Pyke, A.T., Jansen, C.C.,
554 Suhrbier, A., Yakob, L., and Hu, W. (2021). Temperature modulates immune gene expression in
555 mosquitoes during arbovirus infection. Open biology *11*, 200246.
556 40. Dudchenko, O., Batra, S.S., Omer, A.D., Nyquist, S.K., Hoeger, M., Durand, N.C., Shamim, M.S.,
557 Machol, I., Lander, E.S., and Aiden, A.P. (2017). De novo assembly of the Aedes aegypti genome
558 using Hi-C yields chromosome-length scaffolds. Science *356*, 92-95.
559 41. Nora, E.P., Lajoie, B.R., Schulz, E.G., Giorgetti, L., Okamoto, I., Servant, N., Piolot, T., Van Berkum,
560 N.L., Meisig, J., and Sedat, J. (2012). Spatial partitioning of the regulatory landscape of the X-
561 inactivation centre. Nature *485*, 381-385.
562 42. Schoenfelder, S., Furlan-Magaril, M., Mifsud, B., Tavares-Cadete, F., Sugar, R., Javierre, B.-M.,
563 Nagano, T., Katsman, Y., Sakthidevi, M., and Wingett, S.W. (2015). The pluripotent regulatory
564 circuitry connecting promoters to their long-range interacting elements. Genome research *25*, 582-
565 597.
566 43. Qu, J., Betting, V., van Iterson, R., Kwaschik, F.M., and van Rij, R.P. (2022). Chromatin profiling
567 identifies transcriptional readthrough as a conserved mechanism for piRNA cluster biogenesis in
568 mosquitoes. bioRxiv.
569 44. Yoon, Y.J., Kim, J.A., Shin, K.D., Shin, D.-S., Han, Y.M., Lee, Y.J., Lee, J.S., Kwon, B.-M., and Han, D.C.
570 (2011). KRIBB11 inhibits HSP70 synthesis through inhibition of heat shock factor 1 function by
571 impairing the recruitment of positive transcription elongation factor b to the hsp70 promoter.
572 Journal of Biological Chemistry *286*, 1737-1747.
573 45. Neef, D.W., Turski, M.L., and Thiele, D.J. (2010). Modulation of heat shock transcription factor 1 as
574 a therapeutic target for small molecule intervention in neurodegenerative disease. PLoS biology *8*,
575 e1000291.
576 46. Dong, B., Jaeger, A.M., Hughes, P.F., Loiselle, D.R., Hauck, J.S., Fu, Y., Haystead, T.A., Huang, J., and
577 Thiele, D.J. (2020). Targeting therapy-resistant prostate cancer via a direct inhibitor of the human
578 heat shock transcription factor 1. Science Translational Medicine *12*, eabb5647.
579 47. Sanders, H.R., Foy, B.D., Evans, A.M., Ross, L.S., Beaty, B.J., Olson, K.E., and Gill, S.S. (2005). Sindbis
580 virus induces transport processes and alters expression of innate immunity pathway genes in the
581 midgut of the disease vector, Aedes aegypti. Insect biochemistry and molecular biology *35*, 1293-
582 1307.

583 48. Liu, W.-Q., Chen, S.-Q., Bai, H.-Q., Wei, Q.-M., Zhang, S.-N., Chen, C., Zhu, Y.-H., Yi, T.-W., Guo, X.-P.,
584 and Chen, S.-Y. (2020). The Ras/ERK signaling pathway couples antimicrobial peptides to mediate
585 resistance to dengue virus in Aedes mosquitoes. PLoS neglected tropical diseases *14*, e0008660.
586 49. Chen, T.-Y., Lee, Y., Wang, X., Mathias, D., Caragata, E.P., and Smartt, C.T. (2021). Profiling
587 transcriptional response of dengue-2 virus infection in midgut tissue of Aedes aegypti. Frontiers in
588 Tropical Diseases *2*, 708817.
589 50. Howe, M.K., Speer, B.L., Hughes, P.F., Loiselle, D.R., Vasudevan, S., and Haystead, T.A. (2016). An
590 inducible heat shock protein 70 small molecule inhibitor demonstrates anti-dengue virus activity,
591 validating Hsp70 as a host antiviral target. Antiviral research *130*, 81-92.
592 51. Ferreira, P.G., Tesla, B., Horácio, E.C.A., Nahum, L.A., Brindley, M.A., de Oliveira Mendes, T.A., and
593 Murdock, C.C. (2020). Temperature dramatically shapes mosquito gene expression with
594 consequences for mosquito–Zika virus interactions. Frontiers in microbiology *11*, 901.
595 52. Haslbeck, M., Franzmann, T., Weinfurtner, D., and Buchner, J. (2005). Some like it hot: the structure
596 and function of small heat-shock proteins. Nature structural & molecular biology *12*, 842-846.
597 53. Basha, E., Lee, G.J., Breci, L.A., Hausrath, A.C., Buan, N.R., Giese, K.C., and Vierling, E. (2004). The
598 identity of proteins associated with a small heat shock protein during heat stress in vivo indicates
599 that these chaperones protect a wide range of cellular functions. Journal of Biological Chemistry
600 *279*, 7566-7575.
601 54. Vecchi, G., Sormanni, P., Mannini, B., Vandelli, A., Tartaglia, G.G., Dobson, C.M., Hartl, F.U., and
602 Vendruscolo, M. (2020). Proteome-wide observation of the phenomenon of life on the edge of
603 solubility. Proceedings of the National Academy of Sciences *117*, 1015-1020.
604 55. Haslbeck, M., Weinkauf, S., and Buchner, J. (2019). Small heat shock proteins: simplicity meets
605 complexity. Journal of Biological Chemistry *294*, 2121-2132.
606 56. Dabbaghizadeh, A., and Tanguay, R.M. (2020). Structural and functional properties of proteins
607 interacting with small heat shock proteins. Cell Stress and Chaperones *25*, 629-637.
608 57. Scholte, F.E., Tas, A., Martina, B.E., Cordioli, P., Narayanan, K., Makino, S., Snijder, E.J., and van
609 Hemert, M.J. (2013). Characterization of synthetic Chikungunya viruses based on the consensus
610 sequence of recent E1-226V isolates. PloS one *8*, e71047.
611 58. Hahn, C.S., Hahn, Y.S., Braciale, T.J., and Rice, C.M. (1992). Infectious Sindbis virus transient
612 expression vectors for studying antigen processing and presentation. Proceedings of the National
613 Academy of Sciences *89*, 2679-2683.
614 59. Hermanns, K., Marklewitz, M., Zirkel, F., Overheul, G.J., Page, R.A., Loaiza, J.R., Drosten, C., Van Rij,
615 R.P., and Junglen, S. (2020). Agua Salud alphavirus defines a novel lineage of insect-specific
616 alphaviruses discovered in the New World. The Journal of general virology *101*, 96.
617 60. Peleo, J. (1968). Growth of arboviruses in mono-layers from subcultured mosquito embryo cells.
618 Virology *35*, 617-619.
619 61. Marhoul, Z., and Pudney, M. (1972). A mosquito cell line (Mos. 55) from Anopheles gambiae larvae.
620 Transactions of the Royal Society of Tropical Medicine and Hygiene *66*, 183-184.
621 62. van Cleef, K.W., Overheul, G.J., Thomassen, M.C., Kaptein, S.J., Davidson, A.D., Jacobs, M., Neyts, J.,
622 van Kuppeveld, F.J., and van Rij, R.P. (2013). Identification of a new dengue virus inhibitor that
623 targets the viral NS4B protein and restricts genomic RNA replication. Antiviral research *99*, 165-171.
624 63. Andrews, S. (2010). FastQC: a quality control tool for high throughput sequence data. Babraham
625 Bioinformatics, Babraham Institute, Cambridge, United Kingdom.
626 64. Dobin, A., Davis, C.A., Schlesinger, F., Drenkow, J., Zaleski, C., Jha, S., Batut, P., Chaisson, M., and
627 Gingeras, T.R. (2013). STAR: ultrafast universal RNA-seq aligner. Bioinformatics *29*, 15-21.
628 10.1093/bioinformatics/bts635.

629 65. Trapnell, C., Hendrickson, D.G., Sauvageau, M., Goff, L., Rinn, J.L., and Pachter, L. (2013).
630 Differential analysis of gene regulation at transcript resolution with RNA-seq. Nature biotechnology
631 *31*, 46-53.
632 66. Ramírez, F., Dündar, F., Diehl, S., Grüning, B.A., and Manke, T. (2014). deepTools: a flexible platform
633 for exploring deep-sequencing data. Nucleic acids research *42*, W187-W191.
634 67. Love, M.I., Huber, W., and Anders, S. (2014). Moderated estimation of fold change and dispersion
635 for RNA-seq data with DESeq2. Genome Biology *15*, 550. 10.1186/s13059-014-0550-8.
636 68. Kolde, R. (2012). Pheatmap: pretty heatmaps. R package version *1*, 726.
637 69. Szklarczyk, D., Gable, A.L., Nastou, K.C., Lyon, D., Kirsch, R., Pyysalo, S., Doncheva, N.T., Legeay, M.,
638 Fang, T., and Bork, P. (2021). The STRING database in 2021: customizable protein–protein
639 networks, and functional characterization of user-uploaded gene/measurement sets. Nucleic acids
640 research *49*, D605-D612.
641 70. Paysan-Lafosse, T., Blum, M., Chuguransky, S., Grego, T., Pinto, B.L., Salazar, G.A., Bileschi, M.L.,
642 Bork, P., Bridge, A., and Colwell, L. (2023). InterPro in 2022. Nucleic Acids Research *51*, D418-D427.
643 71. Ramírez, F., Bhardwaj, V., Arrigoni, L., Lam, K.C., Grüning, B.A., Villaveces, J., Habermann, B., Akhtar,
644 A., and Manke, T. (2018). High-resolution TADs reveal DNA sequences underlying genome
645 organization in flies. Nature communications *9*, 1-15.
646 72. Zhang, Y., Liu, T., Meyer, C.A., Eeckhoute, J., Johnson, D.S., Bernstein, B.E., Nusbaum, C., Myers,
647 R.M., Brown, M., and Li, W. (2008). Model-based analysis of ChIP-Seq (MACS). Genome biology *9*, 1-
648 9.
649 73. Heinz, S., Benner, C., Spann, N., Bertolino, E., Lin, Y.C., Laslo, P., Cheng, J.X., Murre, C., Singh, H., and
650 Glass, C.K. (2010). Simple combinations of lineage-determining transcription factors prime cis-
651 regulatory elements required for macrophage and B cell identities. Molecular cell *38*, 576-589.
652 74. Varghese, F.S., Thaa, B., Amrun, S.N., Simarmata, D., Rausalu, K., Nyman, T.A., Merits, A.,
653 McInerney, G.M., Ng, L.F., and Ahola, T. (2016). The antiviral alkaloid berberine reduces
654 chikungunya virus-induced mitogen-activated protein kinase signaling. Journal of virology *90*, 9743-
655 9757.
656 75. Reed, L.J., and Muench, H. (1938). A simple method of estimating fifty per cent endpoints.
657 American journal of epidemiology *27*, 493-497.
658 76. Coleman, J., Juhn, J., and James, A.A. (2007). Dissection of midgut and salivary glands from Ae.
659 aegypti mosquitoes. JoVE (Journal of Visualized Experiments), e228.
660 77. Livak, K.J., and Schmittgen, T.D. (2001). Analysis of relative gene expression data using real-time
661 quantitative PCR and the 2− ΔΔCT method. methods *25*, 402-408.

662

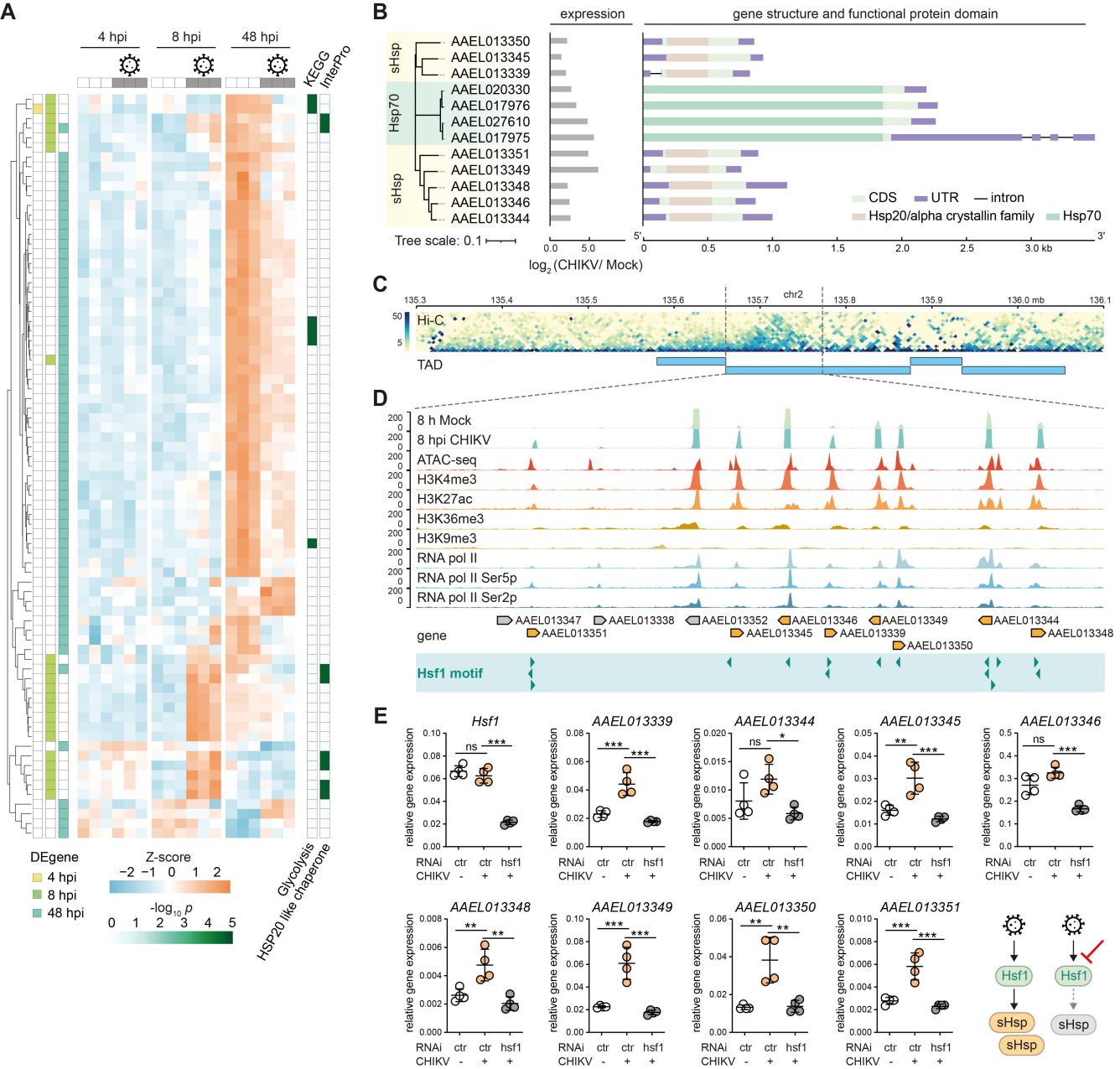
A
4 hpi
8 hpi
48 hpi
KEGG
InterPro
DEgene
4 hpi
8 hpi
48 hpi
Z-score
−2 −1 0 1 2
-log10 p
0 1 2 3 4 5
Glycolysis
HSP20 like chaperone
B
expression
gene structure and functional protein domain
sHsp
Hsp70
sHsp
AAEL013350
AAEL013345
AAEL013339
AAEL020330
AAEL017976
AAEL027610
AAEL017975
AAEL013351
AAEL013349
AAEL013348
AAEL013346
AAEL013344
CDS
UTR
intron
Hsp20/alpha crystallin family
Hsp70
Tree scale: 0.1
0.0 5.0
log2 (CHIKV/ Mock)
5'
3'
0 0.5 1.0 1.5 2.0 2.5 3.0 kb
C
chr2
135.3 135.4 135.5 135.6 135.7 135.8 135.9 136.0 mb 136.1
Hi-C
50
5
TAD
D
8 h Mock
8 hpi CHIKV
ATAC-seq
H3K4me3
H3K27ac
H3K36me3
H3K9me3
RNA pol II
RNA pol II Ser5p
RNA pol II Ser2p
200
0
gene
AAEL013347
AAEL013338
AAEL013352
AAEL013346
AAEL013349
AAEL013344
AAEL013351
AAEL013345
AAEL013339
AAEL013350
AAEL013348
Hsf1 motif
E
Hsf1
AAEL013339
AAEL013344
AAEL013345
AAEL013346
AAEL013348
AAEL013349
AAEL013350
AAEL013351
relative gene expression
RNAi ctr ctr hsf1
CHIKV - + +
ns
*
**
***
Hsf1
sHsp
sHsp

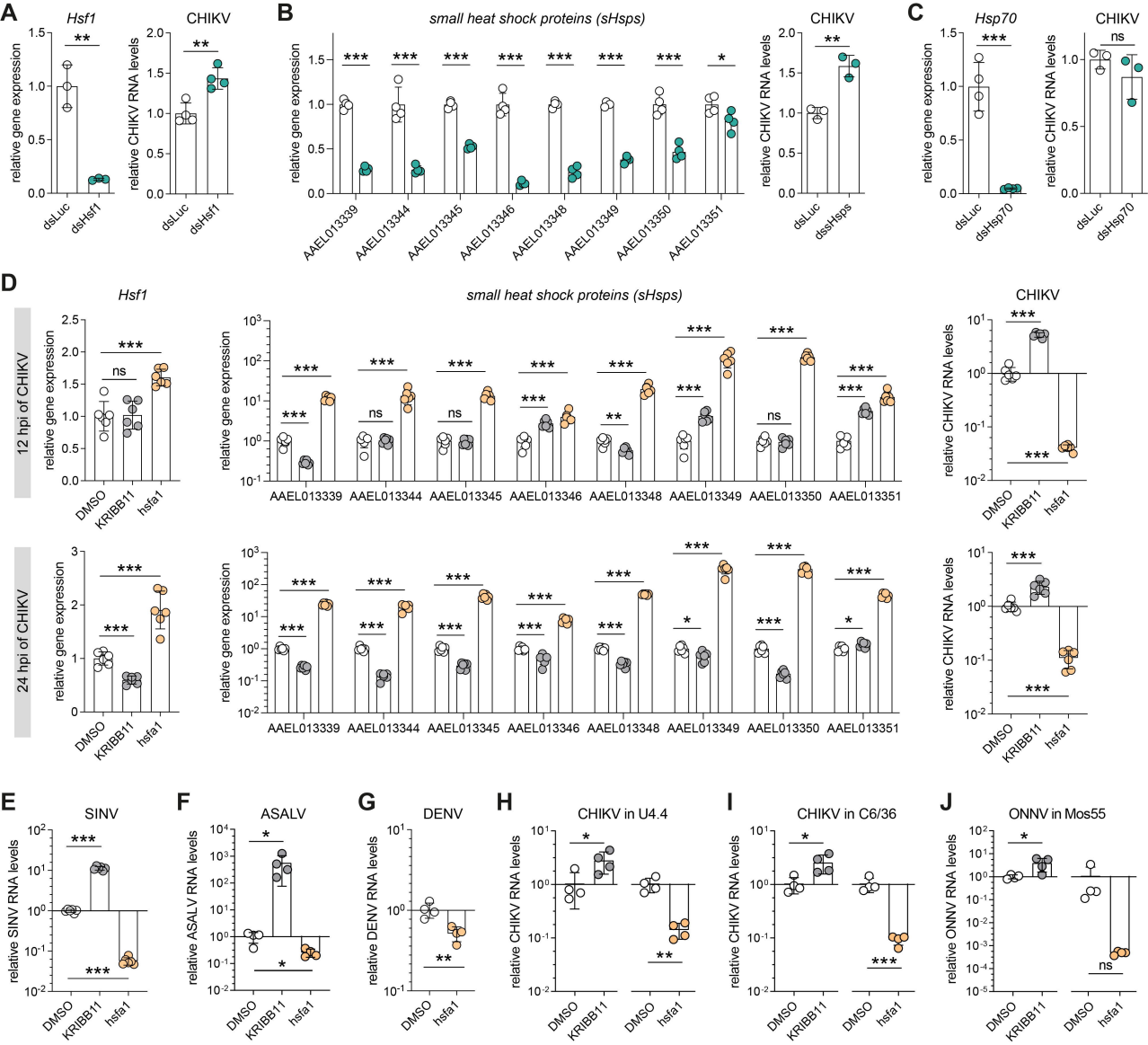
A
Hsf1
CHIKV
relative gene expression
relative CHIKV RNA levels
dsLuc
dsHsf1
B
small heat shock proteins (sHsps)
AAEL013339
AAEL013344
AAEL013345
AAEL013346
AAEL013348
AAEL013349
AAEL013350
AAEL013351
dsHsps
C
Hsp70
dsHsp70
ns
D
12 hpi of CHIKV
24 hpi of CHIKV
DMSO
KRIBB11
hsfa1
E
SINV
relative SINV RNA levels
F
ASALV
relative ASALV RNA levels
G
DENV
relative DENV RNA levels
H
CHIKV in U4.4
I
CHIKV in C6/36
J
ONNV in Mos55
relative ONNV RNA levels

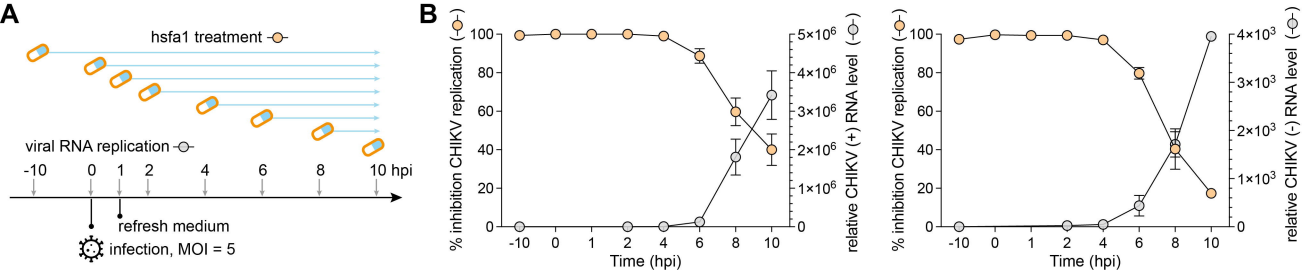
A
hsfa1 treatment
viral RNA replication
-10
0
1
2
4
6
8
10 hpi
refresh medium
infection, MOI = 5
B
% inhibition CHIKV replication (-)
relative CHIKV (+) RNA level
Time (hpi)
% inhibition CHIKV replication (-)
relative CHIKV (-) RNA level
Time (hpi)

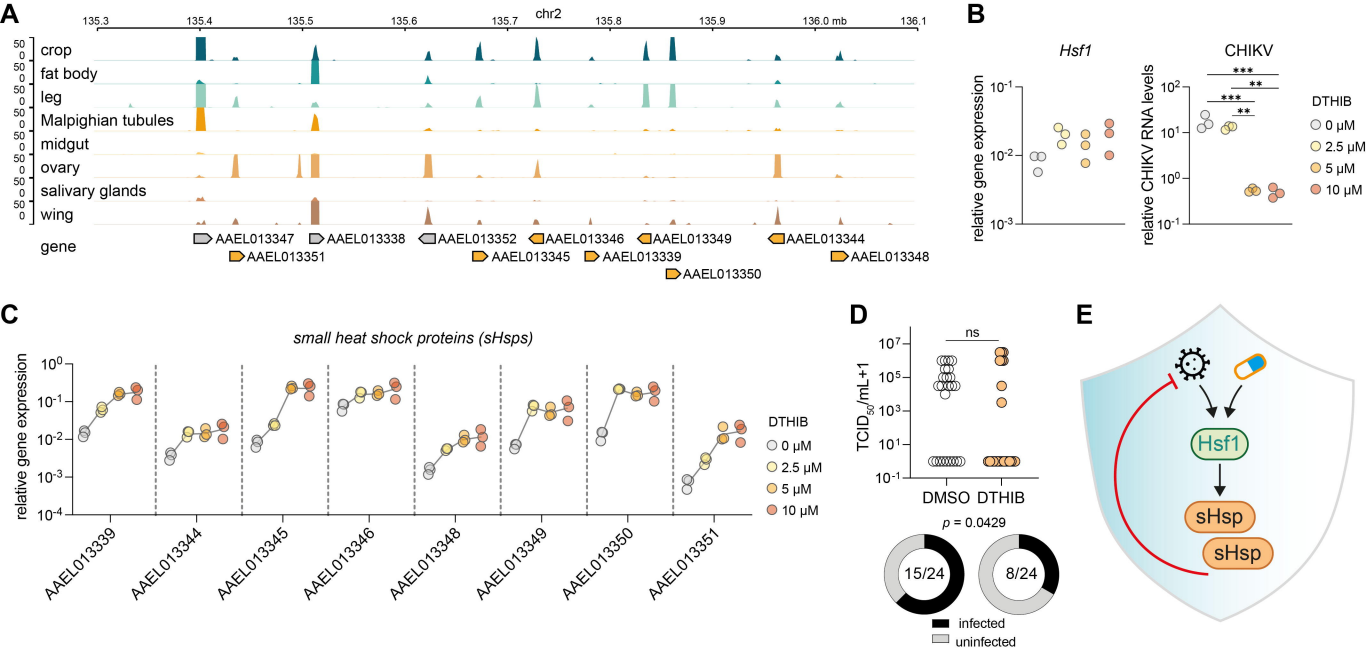
A
chr2
135.3
135.4
135.5
135.6
135.7
135.8
135.9
136.0 mb
136.1
crop
fat body
leg
Malpighian tubules
midgut
ovary
salivary glands
wing
gene
AAEL013347
AAEL013338
AAEL013352
AAEL013346
AAEL013349
AAEL013344
AAEL013351
AAEL013345
AAEL013339
AAEL013348
AAEL013350
B
Hsf1
relative gene expression
CHIKV
relative CHIKV RNA levels
DTHIB
0 μM
2.5 μM
5 μM
10 μM
C
small heat shock proteins (sHsps)
relative gene expression
AAEL013339
AAEL013344
AAEL013345
AAEL013346
AAEL013348
AAEL013349
AAEL013350
AAEL013351
D
ns
TCID50/mL+1
DMSO
DTHIB
p = 0.0429
15/24
8/24
infected
uninfected
E
Hsf1
sHsp
sHsp

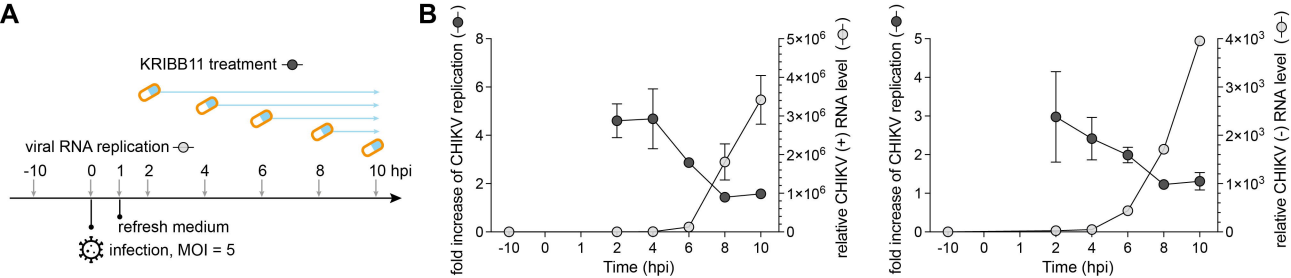
A
KRIBB11 treatment
viral RNA replication
-10
0
1
2
4
6
8
10 hpi
refresh medium
infection, MOI = 5
B
fold increase of CHIKV replication (-)
relative CHIKV (+) RNA level (-)
Time (hpi)
fold increase of CHIKV replication (-)
relative CHIKV (-) RNA level (-)
Time (hpi)

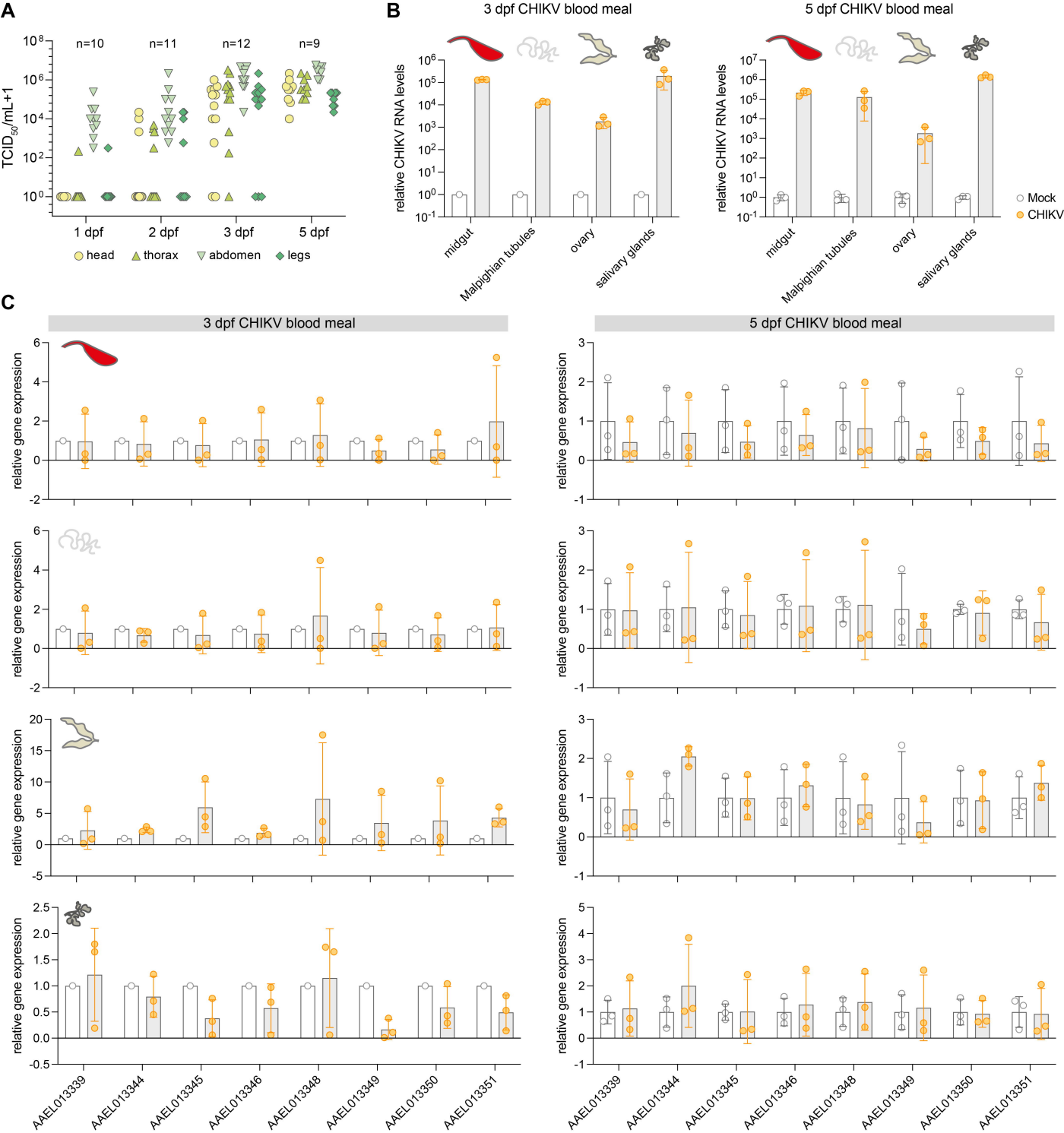
A
n=10
n=11
n=12
n=9
TCID50/mL+1
1 dpf
2 dpf
3 dpf
5 dpf
head
thorax
abdomen
legs
B
3 dpf CHIKV blood meal
5 dpf CHIKV blood meal
relative CHIKV RNA levels
midgut
Malpighian tubules
ovary
salivary glands
Mock
CHIKV
C
3 dpf CHIKV blood meal
5 dpf CHIKV blood meal
relative gene expression
AAEL013339
AAEL013344
AAEL013345
AAEL013346
AAEL013348
AAEL013349
AAEL013350
AAEL013351